RESEARCH ARTICLE | SEPTEMBER 01 1986

Cnoidal standing waves and the transition to the traveling hydraulic jump

Thomas J. Bridges

Phys. Fluids 29, 2819–2827 (1986)
https://doi.org/10.1063/1.865480

Cnoidal standing waves and the transition to the traveling hydraulic jump

Thomas J. Bridges
Mathematics Research Center, University of Wisconsin–Madison, Madison, Wisconsin 53706

(Received 13 January 1986; accepted 1 May 1986)

Standing waves of finite amplitude in an enclosed basin are considered. It is shown that the existing theory of Tadjbakhsh and Keller [J. Fluid Mech. 3, 442 (1960)] breaks down at a critical value of the amplitude dependent upon the depth. By formal perturbation expansion it is found that the solutions change to cnoidal standing waves at this critical value of the amplitude. An experiment is constructed which verifies this theory and also elucidates the wavefield when the amplitude is much larger than the critical amplitude. Based on the experimental observations, a cascade theory is proposed to explain the transition to a traveling hydraulic jump.

I. INTRODUCTION

The two-dimensional periodic solutions of finite amplitude in a rectangular vessel of length $2a$ and still water depth h are considered. The relevant dimensionless parameters (surface tension and viscosity are neglected) for an analysis of waves in a fluid of finite depth are $\delta = h/2a$ and $\epsilon = H/h$, where H is a measure of the wave height. In the limit as $\epsilon \to 0$ the wave height becomes that of a classical standing wave (the sum of two linear progressive waves running in opposite directions). The bifurcations from these solutions (there is an infinite number of linear standing wave modes) for small amplitude ϵ have been found by Tadjbakhsh and Keller.[1] It is shown, however, that their theory breaks down when $\epsilon = O(\delta^2)$. Therefore, the theory of Tadjbakhsh and Keller is valid for all values of the depth but for only a finite range of amplitudes. This is shown by analyzing their results.

By formal perturbation expansion it is shown that the classical standing wave changes to a cnoidal standing wave when $\epsilon = O(\delta^2)$. The cnoidal standing wave is composed of two noninteracting (to first order) progressive cnoidal waves traveling in opposite directions. Unlike the regular (exterior) surface wave problem, where the modulus κ of the cnoidal wave is varied to obtain a family ranging from the cosine wave to the solitary wave, in the interior problem the fixed domain and the periodicity in time fix the value of $\kappa^2 \sim 0.97$. This theory is contained in Sec. II.

This leads to the question of what type of wave occurs for $\epsilon \gg \delta^2$. It is hypothesized that there are no new eigenfunctions in this region. Experimental observations in Sec. III (which are created by including a forcing function) suggest that *compound* cnoidal waves are elicited by the forcing function. First, a compound $1 \oplus 3$ mode wave occurs, and at higher values of ϵ a compound $1 \oplus 3 \oplus 5$ mode wave occurs, and eventually this cascade process results in a traveling hydraulic jump. The results show that at a fixed amplitude the solutions are (apparently) stable, and so the cascade of the higher modes is not dynamic; it occurs in parameter space.

This suggests that the finite amplitude natural frequency of the higher modes become integral multiples of the fundamental in sequence as the amplitude is increased. Much work remains to substantiate these claims, but it does suggest a continuity in parameter space between classical linear standing waves and the traveling hydraulic jump.

In Sec. II the theory of cnoidal standing waves will be derived, and in Sec. III the experimental observations of cnoidal standing waves, the compounding waves observed at larger amplitudes, and the traveling hydraulic jump will be given.

II. THEORY

The independent and dependent variables are scaled in the following way: $x \to 2a$, $y \to h$, $t \to 1/\omega$, $\omega \to \sqrt{gh}/2a$, $\eta \to \epsilon h$, and $\phi \to \epsilon 2a\sqrt{gh}$, where $2a$ is the tank length, h the still water depth, and the dimensionless parameters are $\epsilon = H/h$ and $\delta = h/2a$, where H is a measure of the maximum height of a wave above the still water level. This scaling is appropriate for fluid of finite depth only and must be recast for the case of infinite depth. The governing set of equations and boundary conditions are

$$\delta^2 \frac{\partial^2 \phi}{\partial x^2} + \frac{\partial^2 \phi}{\partial y^2} = 0, \quad \text{for} \quad -\tfrac{1}{2} < x < \tfrac{1}{2}, \quad -1 < y < \epsilon\eta(x,t), \tag{1}$$

$$\frac{\partial \phi}{\partial x} = 0, \quad \text{at} \quad x = \pm\tfrac{1}{2}, \tag{2a}$$

$$\frac{\partial \phi}{\partial y} = 0, \quad \text{at} \quad y = -1, \tag{2b}$$

$$\omega \frac{\partial \eta}{\partial t} + \epsilon \frac{\partial \eta}{\partial x}\frac{\partial \phi}{\partial x} - \frac{1}{\delta^2}\frac{\partial \phi}{\partial y} = 0, \quad \text{on} \quad y = \epsilon\eta(x,t), \tag{3a}$$

$$\omega \frac{\partial \phi}{\partial t} + \frac{\epsilon}{2}\left[\left(\frac{\partial \phi}{\partial x}\right)^2 + \frac{1}{\delta^2}\left(\frac{\partial \phi}{\partial y}\right)^2\right] + \eta = 0, \quad \text{on} \quad y = \epsilon\eta(x,t). \tag{3b}$$

The theory of Tadjbakhsh and Keller is found by expanding the dependent variables ϕ and η and the frequency ω in powers of ϵ in the usual way. The results can be found in their paper. Here we want to show that the solution breaks down when $\epsilon = O(\delta^2)$. The frequency in the limit as $\delta \to 0$ has the expression

$$\lim_{\substack{\delta \to 0 \\ \epsilon\ \text{fixed}}} \omega = \alpha_m + \frac{9\alpha_m}{64\alpha_m^2}\frac{\epsilon^2}{\delta^2} + \cdots, \tag{4}$$

 0031-9171/86/092819-09$01.90

where $\alpha_m = m\pi$, m is the mode number (the results of Tadjbakhsh and Keller are for $m = 1$, and their scaling is slightly different, but the result is the same). We see that the expansion is valid only when $\epsilon \ll \alpha_m \delta$. However, applying the same argument to the wave height results in

$$\lim_{\substack{\delta\to 0\\ \epsilon \text{ fixed}}} \eta(x,t) = \cos\alpha_m \bar{x}\cos t - (3\epsilon/8\alpha_m^2\delta^2)\cos 2\alpha_m\bar{x}\cos 2t$$
$$- (27\epsilon^2/256\alpha_m^4\delta^4)\cos 3\alpha_m\bar{x}\sin 3t + \cdots, \tag{5}$$

where $\bar{x} = x + \frac{1}{2}$. Contrary to the frequency, the wave height expansion breaks down when $\epsilon \sim (\alpha_m\delta)^2$. At this point there is a spillover of the higher harmonics onto the zeroth-order term violating the tenet of the expansion.

A theory is now proposed for the region in the δ-ϵ plane where $\epsilon = O(\delta^2)$. In order for the relation $\epsilon = O(\delta^2)$ to hold δ must be sufficiently small. Therefore, an asymptotic solution is sought with the simultaneous limit $\epsilon\to 0$ and $\delta\to 0$, but with the requirement that ϵ/δ^2 remain constant. This is done by taking the relationship $\delta = \sqrt{\tau\epsilon}$, where $\tau = O(1)$ and carries the sign of ϵ.

The governing equations are (1)–(3) but with the substitution $\delta = \sqrt{\tau\epsilon}$. With ϵ as the only small parameter appearing, a power series solution in ϵ is sought,

$$\omega = \omega_0 + \epsilon\omega_1 + \epsilon^2\omega_2 + \cdots, \tag{6}$$

$$\eta = \eta_0 + \epsilon\eta_1 + \epsilon^2\eta_2 + \cdots, \tag{7a}$$

$$\phi = \phi_0 + \epsilon\phi_1 + \epsilon^2\phi_2 \cdots. \tag{7b}$$

These expressions are substituted into the governing equations and boundary conditions, the free surface boundary conditions are expanded in a Taylor series about the still water level, and terms proportional to like powers of ϵ are set to zero resulting in a sequence of boundary value problems. The Laplace equation gives

$$\phi_0 = \psi_0(x,t), \tag{8}$$

$$\phi_1 = \psi_1(x,t) - \frac{\tau}{2}(1+y)^2\frac{\partial^2\psi_0}{\partial x^2}, \tag{9}$$

$$\phi_2 = \psi_2(x,t) - \frac{\tau}{2}(1+y)^2\frac{\partial^2\psi_1}{\partial x^2} + \frac{\tau^2}{24}(1+y)^4\frac{\partial^4\psi_0}{\partial x^4}, \tag{10}$$

etc. These may then be substituted into the free surface boundary conditions. The zeroth-order problem is then

$$\eta_0 + \omega_0\frac{\partial\psi}{\partial t} = 0, \tag{11}$$

$$\omega_0\frac{\partial\eta_0}{\partial t} + \frac{\partial^2\psi_0}{\partial x^2} = 0, \tag{12}$$

and the first-order problem is

$$\eta_1 + \omega_0\frac{\partial\psi_1}{\partial t} - \frac{\omega_0\tau}{2}\frac{\partial^3\psi_0}{\partial x^2\partial t} + \omega_1\frac{\partial\psi_0}{\partial t} + \frac{1}{2}\left(\frac{\partial\psi_0}{\partial x}\right)^2 = 0, \tag{13}$$

$$\omega_0\frac{\partial\eta_1}{\partial t} + \frac{\partial^2\psi_1}{\partial x^2} - \frac{\tau}{6}\frac{\partial^4\psi_0}{\partial x^4} + \omega_1\frac{\partial\eta_0}{\partial t} + \frac{\partial\eta_0}{\partial x}\frac{\partial\psi_0}{\partial x} + \eta_0\frac{\partial^2\psi_0}{\partial x^2} = 0, \tag{14}$$

and this may be continued to higher order. Here the solution will be carried through the first order.

Combining (11) and (12), the zeroth-order problem is a homogeneous wave equation,

$$\Box\psi_0 = 0, \tag{15}$$

where $\Box$ is the D'Alembertian

$$\Box \equiv \omega_0^2\frac{\partial^2}{\partial t^2} - \frac{\partial^2}{\partial x^2}, \tag{16}$$

with the additional requirement that $\partial\psi_0/\partial x$ vanish on the vertical boundary $x = \pm\frac{1}{2}$. Equation (15) and the wall boundary condition have the general solution

$$\omega_0 = \alpha_m, \tag{17}$$

$$\psi_0 = f(\xi) + f(\chi), \tag{18}$$

where $\xi = t + \alpha_m\bar{x}$, $\chi = t - \alpha_m\bar{x}$, $\alpha_m = m\pi$, and $\bar{x} = x + \frac{1}{2}$. With (11) the zeroth-order wave height is found to be

$$\eta_0 = -\alpha_m[f'(\xi) + f'(\chi)]. \tag{19}$$

The function $f(\xi)$ is, however, unknown at this order. The Fredholm solvability condition applied at the next order will result in an expression for $f(\xi)$.

The zeroth-order results (17) and (18) are substituted into (13) and (14). The two equations are combined to form the following inhomogeneous wave equation for ψ_1,

$$\Box\psi_1 = F_1(x,t), \tag{20}$$

where

$$\begin{aligned} F_1(x,t) = {} & (\tau\alpha_m^4/3)\{f''''(\xi) + f''''(\chi)\} \\ & - 2\alpha_m\omega_1\{f''(\xi) + f''(\chi)\} \\ & - 3\alpha_m^3\{f'(\xi)f''(\xi) + f'(\chi)f''(\chi)\} \\ & + \alpha_m^3\{f''(\xi)f'(\chi) + f'(\xi)f''(\chi)\}. \end{aligned} \tag{21}$$

Equation (20) has a solution only if $F_1(x,t)$ satisfies

$$\int_0^{2\alpha_m} F_1\left[\frac{\xi-\chi}{2\alpha_m}, \frac{\xi+\chi}{2}\right] d\xi = 0. \tag{22}$$

This is a variant of the Fredholm alternative and is proved in Appendix A. Application of this requirement results in the following nonlinear ordinary differential equation for f,

$$(\tau\alpha_m^4/3)f''''(\chi) - 2\alpha_m\omega_1 f''(\chi) - 2\alpha_m^3 f'(\chi)f''(\chi) = 0. \tag{23}$$

Defining $h(\chi) = -\alpha_m f'(\chi)$ and integrating the equation once,

$$\tau h''(\chi) - \frac{6\omega_1}{\alpha_m^3}h(\chi) + \frac{9}{2\alpha_m^2}h^2(\chi) - \frac{9}{4\alpha_m^3}I_1 = 0. \tag{24}$$

Conservation of mass requires $\int_0^{2\alpha_m} h(x)dx = 0$; therefore, I_1 is a positive definite constant given by

$$I_1 = \int_0^{2\alpha_m} h^2(x)dx. \tag{25}$$

It is important to note that the *nonlinearity* of the resulting expression for $h(\chi)$ is *quadratic*. This suggests that the nonlinearity of the operator is quadratic in that region of the δ-ϵ plane where $\epsilon = O(\delta^2)$ (and this may also be true for $\epsilon \gg \delta^2$

as suggested by the work of Chester[2]). It may be shown that the operator for $\epsilon \ll \delta^2$ is *cubic* in the nonlinearity in the neighborhood of the bifurcation points.

The solution of (24) can be found in terms of Jacobian elliptic functions, i.e.,

$$h(\chi) = A + B\,\mathrm{cn}^2(\chi;\kappa), \tag{26}$$

when $\omega_1 = \frac{3}{2}\alpha_m A - \frac{2}{3}\tau\alpha_m^3(1-2\kappa^2)$, and

$$A = -\tfrac{4}{3}\alpha_m^2\tau\{\kappa^2 - 1 + (1/\pi)E(\pi;\kappa)\}, \tag{27}$$

$$B = \tfrac{4}{3}\kappa^2\tau\alpha_m^2, \tag{28}$$

and the constant I_1 is found to have the following expression:

$$I_1 = 2\alpha_m A^2 - (8\omega_1/3)A + \tfrac{8}{9}\tau\alpha_m^3 B(1-\kappa^2). \tag{29}$$

The $\mathrm{cn}(\chi;\kappa)$ is the family of cnoidal functions with modulus κ. Necessary details for this and the other Jacobian elliptic functions are found in Byrd and Friedman.[3] Here $f(\chi)$ is found by integrating $h(\chi)$:

$$f(\chi) = -\tfrac{4}{3}\tau\alpha_m\kappa^2 Z(\chi;\kappa) + \text{const}, \tag{30}$$

where $Z(\chi;\kappa)$ is the Jacobian zeta function. The constant is arbitrary and it is chosen for convenience to be zero to satisfy $\int_0^{2\alpha_m} f(\chi)\,d\chi = 0$. A complete description of the zeroth-order solution may now be given:

$$\omega_0 = \alpha_m, \tag{31}$$

$$\phi_0(x,t) = -\tfrac{4}{3}\tau\alpha_m\kappa^2[Z(t+\alpha_m\bar{x};\kappa) + Z(t-\alpha_m\bar{x};\kappa)], \tag{32}$$

$$\eta_0(x,t) = -\tfrac{8}{3}\alpha_m^2\tau[\kappa^2 - 1 + (1/\pi)E(\pi;\kappa)] + \tfrac{4}{3}\kappa^2\tau\alpha_m^2 \times [\mathrm{cn}^2(t+\alpha_m\bar{x};\kappa) + \mathrm{cn}^2(t-\alpha_m\bar{x};\kappa)], \tag{33}$$

and the first-order correction to the frequency is found to be

$$\omega_1 = -2\tau\alpha_m^3[(1/\pi)E(\pi;\kappa) - \tfrac{1}{3}(2-\kappa^2)], \tag{34}$$

which is positive. Therefore, the bifurcation is supercritical, i.e., the natural frequency increases with increasing amplitude.

The zeroth-order wave height can be cast in another illuminating form. The cn^2 function has the following cosine series [when $K(\pi/2;\kappa) = \pi$]:

$$\mathrm{cn}^2(x;\kappa) = \sum_{n=0}^{\infty} c_n \cos nx, \tag{35}$$

where

$$c_0 = (1/\kappa^2)\,[E(\pi;\kappa)/\pi + \kappa^2 - 1], \tag{36a}$$

and

$$c_n = (2/\kappa^2)\,[nq^n/(1-q^{2n})], \quad \text{for } n>0, \tag{36b}$$

where $q = \exp[-K(\pi/2;\sqrt{1-\kappa^2})]$. Substituting this into (33), it is found that η_0 has the following cosine series:

$$\eta_0(x,t) = \tfrac{8}{3}\kappa^2\tau\alpha_m^2 \sum_{n=1}^{\infty} c_n \cos n\alpha_m\bar{x}\cos nt, \tag{37}$$

with c_n given in (36b).

With $f(\chi)$ known, it may be substituted into the right-hand side of (20), and upon integration the first-order solution for ψ_1 is found to be

$$\psi_1 = -(I_1/2\alpha_m^2)(\xi+\chi) + (\alpha_m/4)[f(\xi)f'(\chi) + f(\chi)f'(\xi)] + [f_1(\xi) + f_1(\chi)], \tag{38}$$

and after combining this with (9) the complete expression for the first-order potential is

$$\phi_1 = -(I_1/2\alpha_m^2)(\xi+\chi) + (\alpha_m/4)[f(\xi)f'(\chi) + f(\chi)f'(\xi)] + (\tau/2)\alpha_m(1+y)^2 \times [h'(\xi) + h'(\chi)] + [f_1(\xi) + f_1(\chi)], \tag{39}$$

and with (13) the first-order wave height is

$$\eta_1 = \frac{I_1}{2\alpha_m} + \frac{\omega_1}{\alpha_m}\left(h(\xi) + h(\chi) - \frac{1}{2}h(\xi)h(\chi) - \frac{\alpha_m^2\tau}{2}[h''(\xi) + h''(\chi)]\right) + (\alpha_m/4) \times [f(\xi)h'(\chi) + f(\chi)h'(\xi)] - \tfrac{1}{2}[h(\xi) - h(\chi)]^2 - \alpha_m[f_1'(\xi) + f_1'(\chi)]. \tag{40}$$

The function $f_1(\xi)$, as well as the second-order correction to the frequency, may be found by imposing the Fredholm solvability condition to the second-order problem.

The main result is that the zeroth-order wave height is given by a family of left- and right-running cnoidal waves with parameter κ varying over $0 \leqslant \kappa^2 \leqslant 1$. The combination of the left-running and right-running waves forms a standing cnoidal wave. If $\kappa^2 = 1$, then $\mathrm{cn}(\xi;1) \to \mathrm{sech}(\xi)$, which would then suggest that the waves would be a combination of a right- and left-running solitary wave. However, this is not the case since the solitary wave, because of the necessity of an infinitely long tail, will not satisfy the periodicity condition. In fact if it is required that the solution be periodic in time with period 2π, then there is only one member of the κ family which will satisfy this. The $\mathrm{cn}^2(\xi;\kappa)$ function is periodic with period $2K(\pi/2;\kappa)$, where $K(\pi/2;\kappa)$ is the complete elliptic integral of the first kind. Therefore the admissible value of κ is given by the root of the transcendental equation

$$\pi = \int_0^{\pi/2} \frac{d\zeta}{\sqrt{1-\kappa^2\sin^2\zeta}} = 0. \tag{41}$$

A numerical solution of this equation results in a value for κ^2 of $\kappa^2 \sim 0.9691$.

The second-order frequency correction ω_2 and the function $f_1(\chi)$ may be found through application of the solvability condition on the second-order problem. The second-order problem has the form

$$\eta_2 + \omega_0\frac{\partial\phi_1}{\partial t} + \omega_2\frac{\partial\phi_0}{\partial t} + \frac{\partial\phi_0}{\partial x}\frac{\partial\phi_1}{\partial x} + \frac{1}{2\tau}\left(\frac{\partial\phi_1}{\partial y}\right)^2 + \omega_0\eta_0\frac{\partial^2\phi_1}{\partial y\,\partial t} = 0 \tag{42}$$

and

$$\omega_0\frac{\partial\eta_2}{\partial t} - \frac{1}{\tau}\frac{\partial\phi_3}{\partial y} + \omega_1\frac{\partial\eta_1}{\partial t} + \omega_2\frac{\partial\eta_0}{\partial t} + \frac{\partial\eta_0}{\partial x}\frac{\partial\phi_1}{\partial x} + \frac{\partial\eta_1}{\partial x}\frac{\partial\phi_0}{\partial x} - \frac{\eta_0}{\tau}\frac{\partial^2\phi_2}{\partial y^2} - \frac{\eta_1}{\tau}\frac{\partial^2\phi_1}{\partial y^2} = 0. \tag{43}$$

When these equations are combined and the solvability condition is applied, after some integration and algebraic manipulation the resulting differential equation for $f_1(\chi)$ is

$$\tau f_1'''(\chi) - \frac{6\omega_1}{\alpha_m^3} f_1'(\chi) + \frac{9}{2\alpha_m^2} h(\chi) f_1'(\chi)$$
$$= \text{const} + \left(\frac{6\omega_2}{\alpha_m^4} + \frac{3I_1}{4\alpha_m^4} + \frac{4\tau d_1}{15\alpha_m} - \frac{57\omega_1^2}{5\alpha_m^5}\right) h(\chi)$$
$$- \frac{5\tau d_2}{2\alpha_m} h^2(\chi) - \frac{2\tau}{\alpha_m} h'(\chi) h'(\chi), \tag{44}$$

where the numbers d_1 and d_2 are given in Appendix B, and the integration constant is chosen such that the integral of $f_1(\chi)$ is zero. The equation is a linear differential equation with nonconstant coefficients which has the homogeneous solution $f_{1h}'(\chi) = \beta h(\chi)$, where β is an arbitrary constant. The inhomogeneous part must satisfy an additional solvability condition. After multiplication of (44) by $h(\chi)$ and integration from 0 to $2\alpha_m$ the left-hand side is zero and the integral of the right-hand side results in an expression for ω_2:

$$\omega_2 = -\frac{1}{8} I_1 - \frac{2}{45} d_1 \alpha_m^3 + \frac{57\omega_1^2}{30\alpha_m} + \frac{\tau \alpha_m^3}{12 I_1} (5 d_2 I_4 - 2 I_5), \tag{45}$$

where the constants d_1, d_2, I_4, and I_5 are given in Appendix B. After substitution of this into (44) it can be shown that (44) has the general solution

$$f_1'(\chi) = A_1 + A_2 h(\chi) + (4/7\alpha_m) h^2(\chi). \tag{46}$$

The arbitrariness of A_1 is due to the integration constant in (44), and the arbitrariness of A_2 is due to the homogeneous solution of (44). This arbitrariness, however, may be eliminated. To satisfy conservation of mass the integral of $f_1'(\chi)$ in 0 to $2\alpha_m$ must be zero; therefore,

$$A_1 = -2I_1/7\alpha_m^2, \tag{47}$$

and if ϵ is defined such that it is proportional to the leading order wave height, then the inner product of η_0 with η_1 should be zero. This gives a value for A_2 of

$$A_2 = -2\,\omega_1/\alpha_m^2 + 33 I_4/7 I_1 \alpha_m. \tag{48}$$

A complete description for the first-order solution has now been found.

In Fig. 1 a bifurcation diagram for the frequency is shown. Here ω_1 is positive definite and it appears that ω_2 is as well so the bifurcation is supercritical for all the modes; the natural frequency of the cnoidal standing waves increases with increasing amplitude, but this is vague because the depth is changing as well. A typical time series for the wave height at the left tank wall is given in Fig. 2.

In Fig. 3, the evolution of the mode $m = 1$ cnoidal standing wave is shown. The result is plotted as a function of space with each successive frame $\frac{1}{20}$th of a temporal period. This wave is very similar to that found by Vanden-Broeck and Schwartz,[4] using a numerical technique, and shown in their Fig. 3. Figure 4 shows the evolution of a 2 mode. The "traveling character" of these waves is to be contrasted with the "standing character" of the standing waves found by Tadjbakhsh and Keller (TK). In Fig. 5 the evolution of a 1 mode TK standing wave is plotted. Here the wave appears to move vertically and otherwise remain a coherent "slosh" wave.

The distribution of the 2 mode at $t = \pi$ at the bottom of Fig. 4 raises an interesting question about the enclosed angle of the crest of a large amplitude cnoidal standing wave. It is well known that the Stokes wave has a limiting angle of 120°. Schwartz and Whitney[5] have shown that the nonlinear classical standing wave probably has a limiting angle of 90°. The cnoidal standing wave appears to have a limiting angle less than 90°, probably much less than 90°, and possibly a limiting configuration that is a cusp.

Using a two-timing method Rogers and Mei (their work is summarized in Mei[6]) have also shown that when the amplitude and dispersion are balanced the resulting standing wave is composed of two noninteracting cnoidal waves traveling in opposite directions (to leading order). Although their procedure is slightly different, the result is essentially the same. In addition to the above result they take τ (related to the Ursell number) to be a function of κ. However, τ must be of order unity for a consistent theory; consequently, the

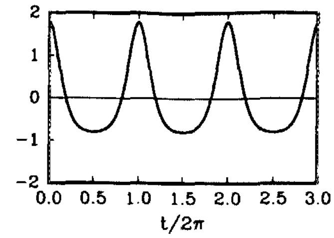

FIG. 2. Time series for the wave height at the left tank wall for a cnoidal standing wave.

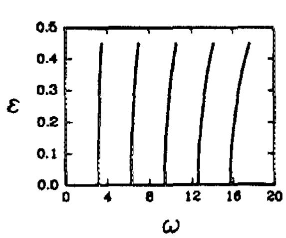

FIG. 1. Bifurcation diagram for the natural frequency (the first five modes) of standing cnoidal waves.

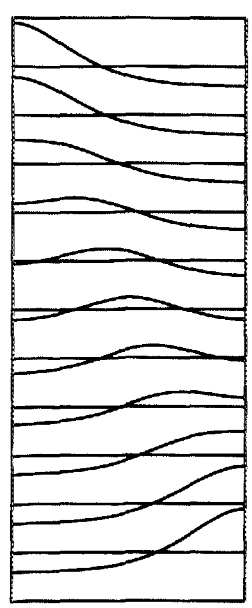

FIG. 3. Temporal evolution of the x distribution of the wave height for a 1-mode cnoidal standing wave.

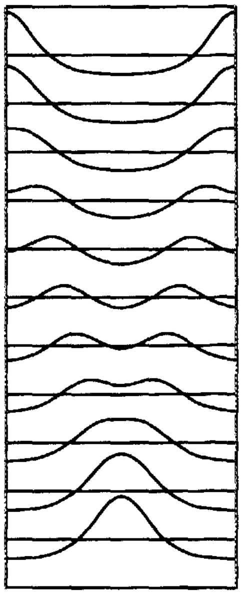

FIG. 4. Temporal evolution of the x distribution of the wave height for a 2-mode cnoidal standing wave.

allowable range of values will result in qualitatively similar cnoidal standing waves. This fact is illustrated by comparing Fig. 3 above and Fig. 6.1, p. 553 of Mei,[6] which are quite similar.

III. EXPERIMENTAL OBSERVATIONS

An experiment was constructed to verify the theory of cnoidal waves and to elucidate the region where $\epsilon \gg \delta^2$. A $\frac{1}{4}$ in. thick Plexiglas tank was constructed of tank length $2a = 18$ in., breadth = 3 in., and tank height = 15 in. The linear natural frequencies in Hz of this tank as a function of δ are

$$f_m \sim 1.307 \sqrt{m \tanh m\pi\delta}, \quad \text{for } m = 1,2,3,\ldots .$$

The physical layout of the experiment is depicted in Fig. 6. It is important to note that in a rigid-walled tank undergoing forced harmonic oscillations only *odd* modes may be excited.

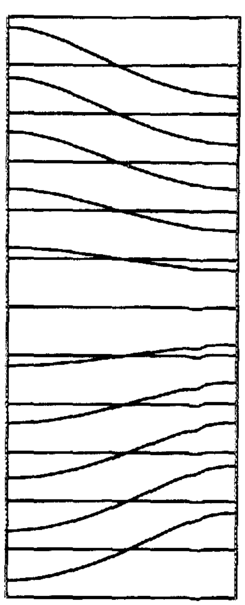

FIG. 5. Temporal evolution of the x distribution of the wave height for a 1-mode Tajdbakhsh and Keller standing wave.

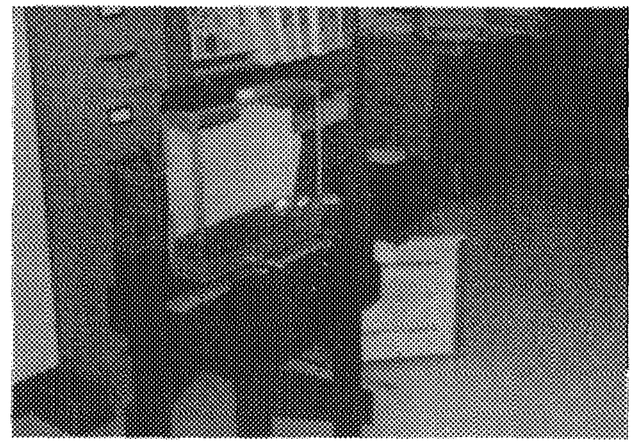

FIG. 6. Experimental setup for the study of waves in a rectangular basin. The black object in background is the vertical oscillator, and the electronics to the left process the measured wave height.

In fact it appears that the only way to excite even modes is to move the endwalls harmonically. This is how Taylor[7] excited standing waves (in his case the $m = 2$ mode) in his study of the limiting configuration of standing waves in deep water.

A horizontal steel shaft, rigidly bolted to the bottom center of the tank and mounted in rotary bearings on a wooden support stand, acts as the pivot for the roll motion of the tank. A driving arm, attached perpendicular to the shaft, is connected to the driving mechanism, which oscillates vertically. With this arrangement the vertical oscillation of the driving mechanism imparts an angular rotation to the tank, i.e., roll motion about the bottom center of the tank. The driving mechanism is a Bruel & Kjaer Vibration Exciter Type 4808.

The harmonic output to the driving mechanism is created in and controlled by an HP 5451C Fourier analyzer. The programmable Fourier analyzer is used to create and output a time series to the exciter. The amplitude of the exciter is controlled in real time and can be continuously varied. On command the Fourier analyzer receives and processes the time series for the wave height. The wave height is measured using a taut wire capacitance wave guage mounted 1 in. from the left tank wall.

Experiments on waves of this type appear to have been initiated by Taylor in his study of standing waves where the walls (and hence the domain) were oscillated harmonically. The approach used in this work where a rigid walled tank is set in harmonic motion has been used in many NASA experiments. A summary of the early work is given in Abramson.[8] In the experiment the wave forms are elicited by forcing the tank to oscillate. Therefore, there is not complete congruence between the solutions observed and a bifurcation analysis. However, when the forcing frequency is near resonance, the solution of the forced problem should be very near that of the bifurcation analysis. Therefore, the forcing frequency will be near resonance unless otherwise noted. For a particular run, once the depth is fixed, the only parameters are the frequency f and the amplitude of the forcing function. In addition the physical experiment is performed with a vis-

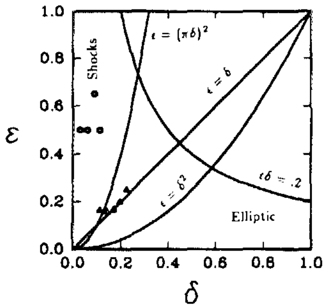

FIG. 7. A diagram of the δ-ϵ plane which shows approximately where the values of ϵ for fixed δ where standing waves were no longer observed, and the circles represent the lowest values of ϵ for fixed δ where a traveling hydraulic jump was observed.

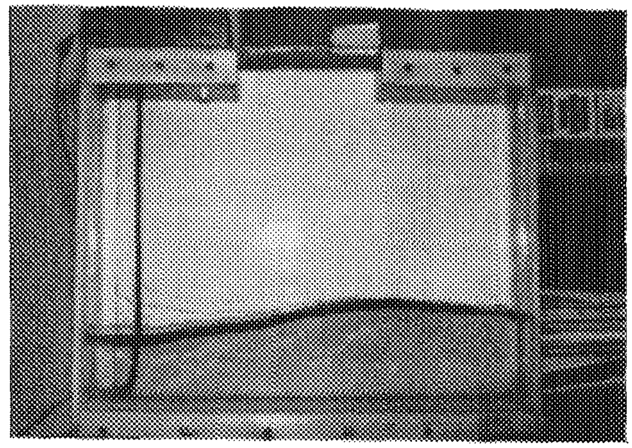

FIG. 9. A 1-mode cnoidal standing wave at a different time with $\delta \sim 0.2$, $f_1 = 0.97$, and $f = 1.0$.

cous fluid (although very small viscosity), and the theory is for an ideal fluid. However the interest is in translation invariant *periodic* solutions. The viscosity will have minimal qualitative effect on this type of wave and contribute only a small perturbation to the amplitude.

The regimes in the experiment are broken down in Fig. 7 where a rough diagram of the waves observed for various combinations of ϵ and δ is plotted. The points near the diagonal are the observed values of ϵ, for fixed δ, where pure standing waves were observed to break down. Above these points the waves observed were compound waves. Curves of $\epsilon = \delta$, $\epsilon = \delta^2$ as well as $\epsilon = (\pi\delta)^2$ are superimposed on the diagram. It is seen that the breakdown of standing waves occurs at $\epsilon \sim \delta$ or equally well at $\epsilon \sim (\pi\delta)^2$. There is then an intermediate region where compound waves are observed and then when $\epsilon >$ *about* $\frac{1}{2}$ and $\delta <$ *about* 0.15 the traveling hydraulic jump is observed exclusively. Although the traveling jump is three dimensionally unsteady in a strict sense, in the large it is essentially two dimensional and in fact very stable. Once the hydraulic jump is formed, regardless of how much the amplitude of the tank motion is increased, the jump is maintained with the strength increasing slightly with increasing tank motion. The curve labeled $\epsilon\delta = 0.2$ in the figure is an extrapolation of the result of Schwartz and Whitney.[5] They showed that for fluid of infinite depth (the pure nonlinear classical standing wave), the maximum height of the waveform was reached when $H/2a \sim 0.2$. In terms of ϵ and δ this is $\epsilon \sim 0.2/\delta$, which is superimposed on the figure. This gives an extension of the upper bound for deep water standing waves and may be an upper bound for all types of waves appearing in rectangular vessels. The intersection of this curve with the $\epsilon = \delta^2$ curve at $\delta \sim 0.6$ suggests that for $\delta > 0.6$ the only class of existing waves is the classical standing waves.

The first experimental result is a verification of cnoidal standing waves. Choosing $\delta \sim 0.2$ and the forcing frequency $f = 1$ Hz, which is just above the linear natural frequency, photographs were taken at three stages of the evolution. These are shown in Figs. 8–10. The wave has the distinct undulating motion associated with the cnoidal standing wave and not observed in the usual standing wave, which has (almost) a node at the center of the tank. Comparing these three figures with Fig. 3 it is seen that 8 resembles the theoretical evolution at $t =$ (9 or 10) $(\pi/10)$, 9 resembles that at $t =$ (6 or 7) $(\pi/10)$, and 10 resembles that at $t = \pi/2$. Figure 11 is an experimentally recorded time series at the left

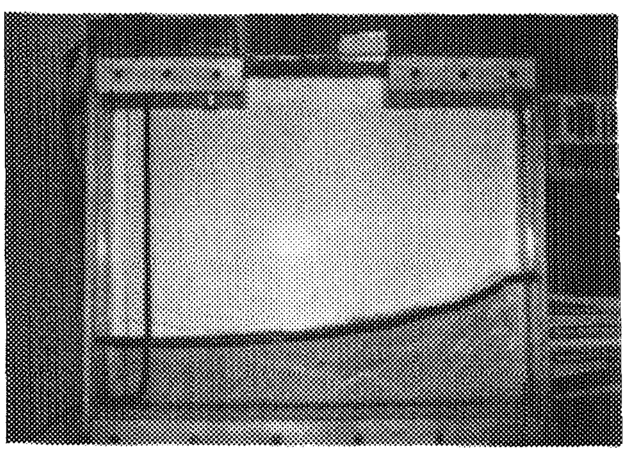

FIG. 8. A 1-mode cnoidal standing wave at peak amplitude when $\delta \sim 0.2$, $f_1 = 0.97$, and $f = 1.0$.

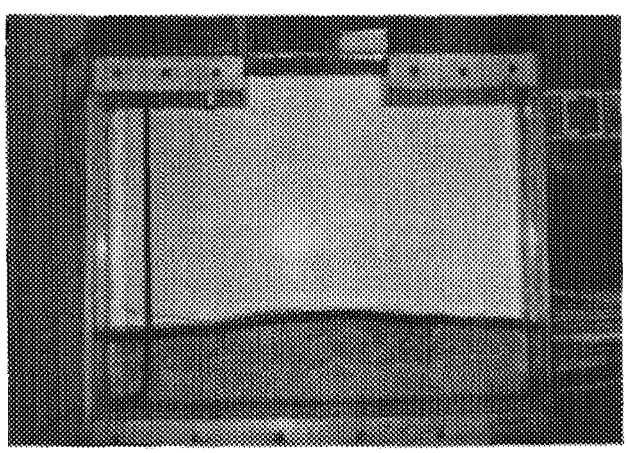

FIG. 10. A 1-mode cnoidal standing wave at a different time with $\delta \sim 0.2$, $f_1 = 0.97$, and $f = 1.0$.

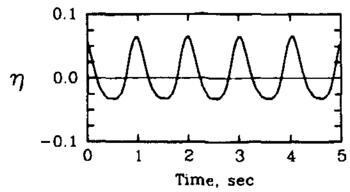

FIG. 11. The time series for the wave height at the left tank wall corresponding to Figs. 8–10. The parameters are $\delta \sim 0.2, f_1 = 0.97$, and $f = 1.0$.

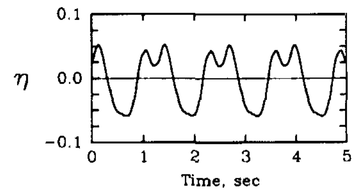

FIG. 13. Time series at the left tank wall for the compound $1 \oplus 3$ standing wave. The parameters are $\delta \sim 0.17, f_1 = 0.91$, and $f = 0.95$.

tank wall for this wave. It compares favorably with the theoretical result in Fig. 2.

We now proceed to investigate the region where $\epsilon \gg \delta^2$. It is possible that there is another class of eigenfunctions between $\epsilon = O(\delta^2)$ and $\epsilon \gg \delta^2$, but this is unlikely. The complex waves observed, as the amplitude increases and the "clean" 1-mode cnoidal standing wave changes into a field with greater spatial complexity, are probably due to the selecting process of the forcing function that is present. Thus rather than a new class of eigenfunctions, these waves are probably compound cnoidal waves, and in fact the observations lend credance to this judgement. There are two distinct compound waves that occur so often that they may be given titles. They are the compound $1 \oplus 3$ wave and the compound $1 \oplus 3 \oplus 5$ wave. The compound $1 \oplus 3$ wave appears at shallow depths but not too shallow and looks like a cnoidal 1 mode joined with a cnoidal 3 mode. Figure 12 is a photograph of a compound $1 \oplus 3$ wave at a particular time. This wave is symmetric. In other words at $\frac{1}{2}$ a period later the waveform is a reflection about the center of the tank. The interesting time series associated with this wave is shown in Fig. 13 and demonstrates the influence of the higher mode. It is important to note that the forcing frequency here is in the neighborhood of the *first* linear natural frequency.

Figures 14(a) and 14(b) are photographic results obtained for the compound $1 \oplus 3 \oplus 5$ wave. Figure 14(a) is a photograph at a particular time, and Fig. 14(b) is at another time. This is a deterministic and periodic wave. The crests seen in these figures move back and forth in the tank at *different speeds*. Thus, although Fig. 14(a) looks like a combination of a $1 \oplus 3$ mode, in Fig. 14(b) it looks more like a 5 mode. The time series for these waves is shown in Fig. 15. It is deterministic and periodic but with many harmonics. In fact Fig. 15(b) is a Fourier transform of the time series in Fig. 15(a), and this shows the rich set of harmonics present. It is interesting to note as well that the compound $1 \oplus 3 \oplus 5$

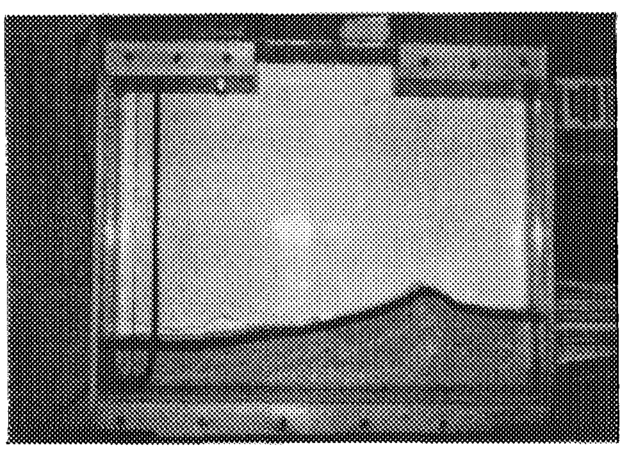

FIG. 12. A photo of the compound $1 \oplus 3$ standing wave. The parameters are $\delta \sim 0.17, f_1 = 0.91$, and $f = 0.95$. Although the forcing function is near the first mode, a 3-mode in space is present.

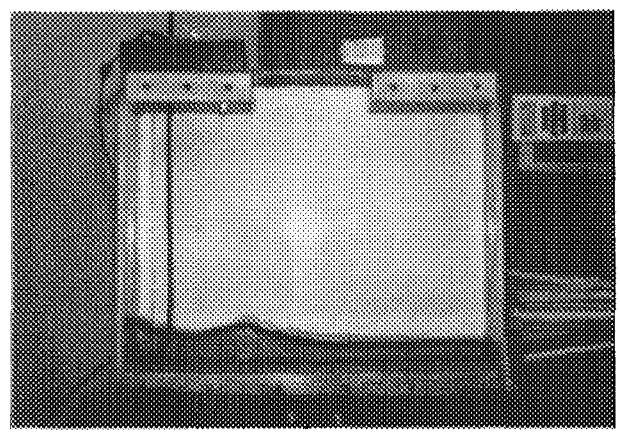

(a)

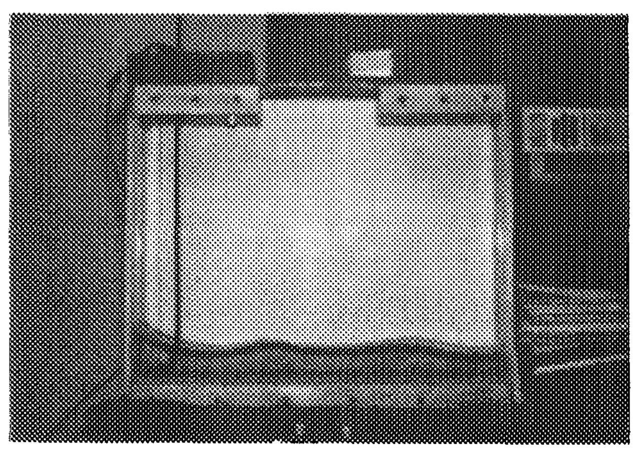

(b)

FIG. 14. A compound $1 \oplus 3 \oplus 5$ wave in shallow water. (a) The parameters are $\delta = 0.084, f_1 = 0.6655$, and $f = 0.67$. (b) The same parameters as (a) at a different time.

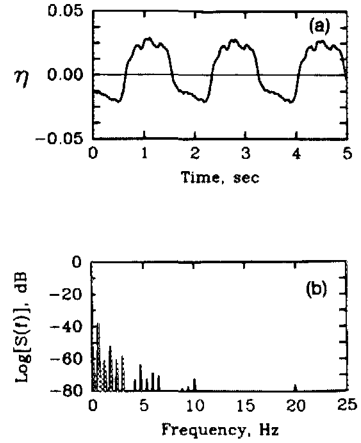

FIG. 15. The wave height at the left tank wall for the compound $1 \oplus 3 \oplus 5$ wave. (a) The time series with parameters of $\delta = 0.098$, $f_1 = 0.716$, and $f = 0.67$. (b) Fourier transform of the time series in Fig. 15(a) showing the richness of the harmonics present.

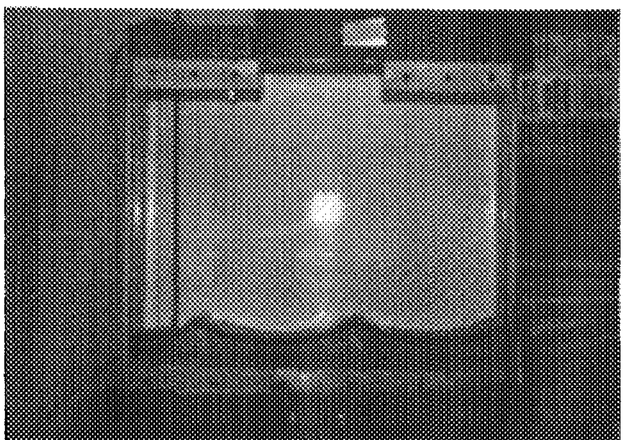

(a)

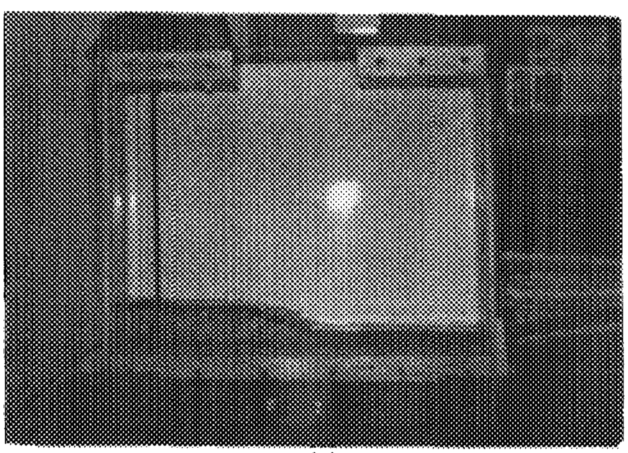

(b)

FIG. 16. Change in type for the wave as the amplitude and frequency change. (a) With $\delta = 0.077$ and $f = f_5 = 2.68$, a 5-mode classical standing wave occurs. (b) However, at the same depth $\delta = 0.077$, but with a lower frequency $f = f_1 = 0.64$ *and sufficiently large amplitude*, a traveling hydraulic jump is formed.

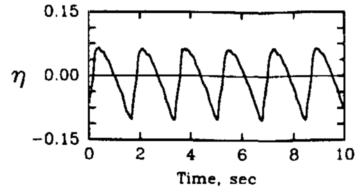

FIG. 17. Time series for a "shallow water" traveling hydraulic jump where $\delta = 0.077$ and $f = f_1 = 0.64$.

wave is always a prelude to the traveling hydraulic jump. If one of these waves is formed and the amplitude of the forcing function is increased further a threshold is reached where the wave changes (bifurcates?) into a traveling hydraulic jump.

For completeness a result for the traveling hydraulic jump is given in Figs. 16(b) and 17. However, Fig. 16(a) is also included to emphasize the role of mode number as well as ϵ and δ. With the fill depth $\delta = 0.077$ and $f \sim f_5 = 2.68$ a 5-mode classical standing wave is formed. However, when the frequency is lowered to $f \sim f_1 = 0.64$ *at sufficient amplitude*, a traveling hydraulic jump is formed, and this is shown in Fig. 16(b) with associated time series in Fig. 17.

These observations lead to the following scenario. When $\epsilon \ll \delta^2$ (and δ small, including the limit as the amplitude goes to zero, i.e., linear waves), an elliptic standing wave forms which bifurcates from the state of rest. This wave is well described by the theory of Tadjbakhsh and Keller. It is a weakly nonlinear wave containing only a few significant harmonics. However, this wave breaks down as ϵ approaches δ^2 in magnitude. By devising a perturbation scheme for small ϵ and δ such that the ratio ϵ to δ^2 is constant, it was shown in Sec. II that a modal family of cnoidal standing waves exists in this region. These waves are much richer harmonically as they have a complete Fourier series.

As the amplitude is increased further the class of solutions are combinations of the set of cnoidal standing waves selected by the forcing function. Observance of this phenomenon in the experiment suggests that as ϵ is increased beyond δ^2 the natural frequencies of the higher mode cnoidal standing waves become integral multiples of the fundamental in sequence. First the 3 mode is excited, and a compound $1 \oplus 3$ mode cnoidal standing wave is formed. As the amplitude is increased further relative to δ^2, a 5 mode is added to the wave, and this forms the compound $1 \oplus 3 \oplus 5$ cnoidal standing wave. Further increase of the amplitude introduces higher and higher harmonics until eventually the wave field jumps to the traveling hydraulic jump.

ACKNOWLEDGMENTS

This work was sponsored in part by the U.S. Army under Contract No. DAAG29-80-C-0041 and by the National Science Foundation under Grant No. DMS-8210950, Mod. 1. The experimental research was made possible through the support of the MIPAC research facility at the Mathematics Research Center.

APPENDIX A: SOLVABILITY CONDITION

In this Appendix a theorem for the solvability of the inhomogeneous wave equation is given. It is an extension of a result first shown by Keller and Ting.[9]

Theorem: *Given the inhomogeneous wave equation,*

$$\omega_0^2 \frac{\partial^2 \Upsilon}{\partial t^2} - \frac{\partial^2 \Upsilon}{\partial x^2} = F(x,t), \quad 0 \leqslant x \leqslant 1, \quad -\infty < t < \infty, \tag{A1}$$

$$\frac{\partial \Upsilon}{\partial x}(0,t) = \frac{\partial \Upsilon}{\partial x}(1,t) = 0, \tag{A2}$$

where $\omega_0 = \alpha_m = m\pi$, *m is any integer greater than zero,* Υ_x, Υ_t, *and F are periodic in time with period* 2π, $F(x,t)$ *is an even function of x, and in addition satisfies*

$$F(x+1, t+\pi) = F(x,t), \tag{A3}$$

then there is a solution to the inhomogeneous problem only if

$$\int_0^{2\alpha_m} F\left[\frac{\xi - \chi}{2\alpha_m}, \frac{\xi + \chi}{2}\right] d\xi = 0. \tag{A4}$$

Proof: Every solution of the homogeneous problem

$$\omega_0^2 \frac{\partial^2 \Psi}{\partial t^2} - \frac{\partial^2 \Psi}{\partial x^2} = 0, \quad 0 \leqslant x \leqslant 1, \quad -\infty < t < \infty, \tag{A5}$$

$$\frac{\partial \Psi}{\partial x}(0,t) = \frac{\partial \Psi}{\partial x}(1,t) = 0, \tag{A6}$$

which is 2π periodic in time and may be expressed as

$$\Psi(x,t) = f(t + \alpha_m x) + f(t - \alpha_m x). \tag{A7}$$

Multiply (A1) by $\Psi(x,t)$ and integrate from 0 to 1 in x and 0 to 2π in t. Integration by parts and the end and periodicity conditions results in the left-hand side becoming zero, then

$$\int_0^{2\pi} \int_0^1 \Psi(x,t) F(x,t) dx\, dt = 0. \tag{A8}$$

For the higher modes, the integrand may be expanded in x taking advantage of the even extension of $F(x,t)$ to all x,

$$\frac{1}{m} \int_0^{2\pi} \int_{-m/2}^{m/2} \Psi(x,t) F(x,t) dx\, dt = 0, \tag{A9a}$$

when m is even and

$$\frac{1}{m} \int_0^{2\pi} \int_{-(m-1)/2}^{(m+1)/2} \Psi(x,t) F(x,t) dx\, dt = 0, \tag{A9b}$$

when m is odd.

Now a change of variables is made to $\xi = t + \alpha_m x$ and $\chi = t - \alpha_m x$. With the change of variables, and use of (A3), and the fact that the integrand is similar in any period parallelogram, the integral (A9) becomes

$$\int_0^{2\alpha_m} \int_0^{2\alpha_m} [f(\xi) + f(\chi)] F\left[\frac{\xi - \chi}{2\alpha_m}, \frac{\xi + \chi}{2}\right] d\xi\, d\chi = 0, \tag{A10}$$

which may be written as the sum of two integrals $f(\xi)F$ and $f(\chi)F$. In the first of these the variables of integration are interchanged. Since F is even in x, the sum becomes

$$2 \int_0^{2\alpha_m} f(\chi) \int_0^{2\alpha_m} F\left[\frac{\xi - \chi}{2\alpha_m}, \frac{\xi + \chi}{2}\right] d\xi\, d\chi = 0. \tag{A11}$$

As a consequence of the arbitrariness of $f(\chi)$, this implies (A4) and proves the theorem.

APPENDIX B: INTEGRALS OF THE ELLIPTIC FUNCTIONS

In this Appendix the details of the Jacobian elliptic functions necessary for the construction of the cnoidal standing wave solutions are given.

The constants d_1, d_2 used in the expression for ω_2 in Sec. II are

$$d_1 = 12\kappa^2 (A^2/B) - 4B(1 - \kappa^2) + 8A(2\kappa^2 - 1), \tag{B1a}$$

$$d_2 = -6\kappa^2 (A/B) - 2(2\kappa^2 - 1), \tag{B1b}$$

where A and B are defined in Sec. II. The integrals used in the first-order solution as well as ω_2 are now given, where $C_p = \int_0^{2\alpha_m} \mathrm{cn}^p(\zeta;\kappa)\, d\zeta$ and $K(\pi/2;\kappa) = \pi$,

$$C_2 = \frac{2\alpha_m}{\kappa^2}\left(\kappa^2 - 1 + \frac{E(\pi;\kappa)}{\pi}\right), \tag{B2a}$$

$$C_4 = \frac{2\alpha_m}{3\kappa^4}\left((2 - 3\kappa^2)(1 - \kappa^2) + 2(2\kappa^2 - 1)\frac{E(\pi;\kappa)}{\pi}\right), \tag{B2b}$$

$$C_6 = \frac{4(2\kappa^2 - 1)C_4 + 3(1 - \kappa^2)C_2}{5\kappa^2}, \tag{B2c}$$

$$C_8 = \frac{6(2\kappa^2 - 1)C_6 + 5(1 - \kappa^2)C_4}{7\kappa^2}, \tag{B2d}$$

and

$$I_2 = \int_0^{2\alpha_m} h'(\zeta) h'(\zeta)\, d\zeta = \frac{8\alpha_m B^2}{15\kappa^4}\left((\kappa^2 - 2)(1 - \kappa^2) + 2(\kappa^4 - \kappa^2 + 1)\frac{E(\pi;\kappa)}{\pi}\right), \tag{B3a}$$

$$\begin{aligned} I_3 &= \int_0^{2\alpha_m} h''(\zeta) h''(\zeta)\, d\zeta \\ &= 4B^2\{2\alpha_m(1 - \kappa^2)^2 + 4(1 - \kappa^2)(2\kappa^2 - 1)C_2 \\ &\quad + [22\kappa^2(\kappa^2 - 1) + 4]C_4 \\ &\quad - 12\kappa^2(2\kappa^2 - 1)C_6 + 9\kappa^4 C_8\}, \end{aligned} \tag{B3b}$$

$$I_4 = \int_0^{2\alpha_m} h^3(\zeta)\, d\zeta = \frac{2\alpha_m^2}{9}\left(\tau I_2 + \frac{6\omega_1}{\alpha_m^3} I_1\right), \tag{B3c}$$

$$I_5 = \int_0^{2\alpha_m} h^2(\zeta) h''(\zeta)\, d\zeta = -\frac{2\alpha_m^2}{9}\left(\tau I_3 + \frac{6\omega_1}{\alpha_m^3} I_2\right). \tag{B3d}$$

[1] I. Tadjbakhsh and J. B. Keller, J. Fluid Mech. **8**, 442 (1960).
[2] W. Chester, Proc. R. Soc. London Ser. A **306**, 5 (1968).
[3] P. F. Byrd and M. D. Friedman, *Handbook of Elliptic Integrals for Engineers and Scientists* (Springer, Berlin, 1971).
[4] J-M. Vanden-Broeck and L. W. Schwartz, Phys. Fluids **24**, 812 (1981).
[5] L. W. Schwartz and A. K. Whitney, J. Fluid Mech. **107**, 147 (1981).
[6] C. C. Mei, *The Applied Dynamics of Ocean Surface Waves* (Interscience, New York, 1983), pp. 550-553.
[7] G. I. Taylor, Proc. R. Soc. London Ser. A **218**, 44 (1953).
[8] H. N. Abramson, NASA Report No. SP-106, 1966.
[9] J. B. Keller and L. Ting, Commun. Pure Appl. Math. **19**, 371 (1966).